Investigation of sol-gel feedstock additions and process variables on the density and microstructure of UN microspheres

JW McMurray[1], RD Hunt[1], TJ Reif[2], GW Helmreich[1], CM Silva[1], RL Seibert[1], TJ Gerczak[1] and KA Terrani[1]

1. *Oak Ridge National Laboratory*
   Oak Ridge, TN 37831
2. *X-Energy, LLC*
   7701 Greenbelt, MD 20770

ABSTRACT

The kernel of fully ceramic microencapsulated (FCM) fuel requires a material with high fissile density. For that reason, among others, UN is the appropriate chemical state for low enriched U fuel. The UN kernels are spheres ~800 micrometer in diameter made using a sol-gel process. The effect of additives on the chemistry and density of the UN microspheres are investigated in this work. Gadolinium nitrate hexahydrate, Gd_2O_3, B, SiO_2 and SiC were incorporated into the sol-gel broth in varying concentrations. It was found that Gd can serve as both a sintering aid and burnable poison when added to the sol-gel broth as a $Gd(NO_3)_36H_2O$. However, even with the increased theoretical density of the UN microspheres, the U density was still too low for the FCM design that replaces UO_2 pellets in a commercial light water reactor. Silicon carbide and B were also successfully added but produced a lower density final product. Other sol-gel processing variables were also investigated. The pour density of the sol-gel feedstock was found to influence the final converted UN kernel density.

1. Introduction

Fully ceramic microencapsulated (FCM) uranium mononitrde (UN) is an accident tolerant fuel (ATF) designed for enhanced safety margins. This is primarily accomplished by delaying and reducing radionuclide release during nuclear accidents. The FCM compact, shown in Fig. 1, is intended to replace the standard UO_2 pellet in a light water reactor (LWR). The UN fuel kernels are encapsulated by tristructural-isotropic (TRISO) layers that are embedded in a dense silicon carbide (SiC) matrix [1, 2] illustrated in Fig. 2. The TRISO coating has been established to be an effective barrier to radionuclide release [3]. The matrix SiC provides additional secondary containment and has been shown to substantially retard steam ingress that results from a breach of cladding event [2].

One challenge to direct substitution of FCM compacts for UO_2 pellets is that much of the U volume is replaced by TRISO coatings and the SiC matrix. Uranium nitride has a heavy metal and theoretical density (TD) of 13.5 and 14.3 g/cc respectively. George et al. [4] show UN is indeed appropriate as the fuel kernel for the FCM design, however the authors identify a technological challenge, that is, the reactivity must be decreased at the beginning of life with a burnable poison, e.g. B, Eu, or Gd. A potential issue for FCM fuel is fission product (FP) attack on the SiC layer of the TRISO coatings during high temperature transients [5-7]. Sacrificial SiC inclusions in the UN kernel itself could mitigate deleterious attack of the TRISO SiC by immobilizing FPs via chemical reaction. Therefore, the focus of this work is to explore the impact of sol-gel feedstock additives and process variables on density and microstructure of UN microspheres after carbothermic reduction and nitriding (CTRN) with the aim of addressing these issues.

Three principal questions drive this study. First, can an additive, in this work SiC, Gd, and B be impregnated into the UN kernel without negatively impacting benchmark density and geometry? Second, what effects do the type of carbon, dispersant, and combination thereof have on the UN after CTRN? It has been observed that the C dispersion influences kernel microstructure with C agglomerations creating pores [5-7]. Lastly, how do the U concentration and gelation temperature, both sol-gel processing variables affect the density in the final product?

2. Experimental

The overall FCM process can be subdivided into three distinct steps as shown in Fig. 3. Feedstock hydrated U bearing spheres with C produced using a sol-gel method are converted to UC_xN_{1-x} by dehydration below ~300°C then carbothermic reduction, occurring in two calcining steps governed by the reactions given in Equations 1 and 2. Subsequent nitriding proceeds via Equation. 3.

$$UO_3 + C \rightarrow UO_2 + 1/2\,C + 1/2\,CO_2 \quad (1)$$

$$UO_2 + (3-2y)C \rightarrow UO_yC_{1-y} + (2-y)CO \quad (2)$$

$$\left(\frac{1-2y-x}{3-2y}\right)UO_2 + \left(\frac{2+x}{3-2y}\right)UO_yC_{1-y} + \left(\frac{1-x}{2}\right)N_2 \rightarrow UC_xN_{1-x} + \left(\frac{xy-2y-2x+2}{3-2y}\right)CO \quad (3)$$

The reaction from Equation 1 occurs over the temperature range of ~300 to ~800°C. From ~1400°C and up, the reaction given by Equation 2 is operative. Finally, at 1900°C, Ar sweep gas is replaced by N_2 to promote the reaction in Equation 3 [8, 9]. The resulting UC_xN_{1-x} kernels are encapsulated with TRISO layers using chemical vapor deposition (CVD) [10-12]. The TRISO particles are then coated with NITE SiC and pressed into fuel compacts [1].

2.1. Sol-gel process

The process to produce hydrated U bearing oxide gel spheres is described in detail in [13-15]. The feedstock for this work uses standard solution concentrations for the hexamethylenetetramine hereafter abbreviated as HMTA (Fisher Scientific) and urea (Fisher Scientific) at 3.2 *M* each. Once prepared and filtered, the density was measured to be 1,140 kg/m^3 and the pH ranged from 8 to 9. Acid deficient uranium nitrate (ADUN) solutions had a density of 1,870 kg/m^3 with a pH of 1.3 and a U concentration of 2.85 *M*. The pH and uranium concentration [15] were used to estimate that the molar ratio of nitrate (NO_3^-) to uranium was approximately 1.65.

In addition to U, HMTA, and urea, each feed solution contained Mogul L or Raven 3500 carbon black (Cabot Corporation) and Tamol SN dispersing agent (Rohm and Haas). Prior to its use, the Mogul L was passed through a 150 mesh sieve to exclude all particles with diameters greater than 105 μm. Enough Mogul L was added to the 113.2 g of the HMTA-urea solution and 3.0 g of distilled water so the carbon to uranium molar ratio in the final feed solution was 2.50−2.65, and 0.08 g of Tamol SN per g of Mogul L was also placed in the HMTA-urea solution. After the B, Gd_2O_3, $Gd(NO_3)_36H_2O$, SiC (Sigma Aldrich), or SiO_2 was added to the HMTA-urea solution and chilled in an ice water bath, the carbon black was dispersed twice using a Hielscher Ultrasound Technology model UP200S ultrasonic probe for 5 min each then cooled in an ice water bath for a minimum of 30 min. This chilled solution was then combined with 159.8 g of ADUN and transferred to a jacketed Pyrex pot that was mounted on a Cimarec 1 magnetic stirrer. The temperature of the feed solution was maintained near 0°C. A "Starburst" stir bar was used to provide continuous mixing of the insoluble particles during each test.

During each feedstock run, the microspheres were collected in a stainless-steel wire-mesh basket. At the end of each test, the basket was lowered into a reservoir with the hot silicone oil for 20 min. After the silicone oil was drained from the gel spheres, the basket was placed in a beaker with a magnetic stir bar and the microspheres were then washed with four successive batches of trichloroethylene (TCE), from J. T. Baker, for a minimum of 15 min. The same equipment used with TCE to remove the residual silicone oil was also used but with 1.5 *M* NH_4OH to remove the NH_4NO_3, urea, and unreacted HMTA from the microspheres. Without C present, NH_4OH concentrations are typically 0.5. For sol-gel with C, higher NH_4OH concentration is needed to significantly reduce C losses to the wash solutions. Each NH_4OH wash lasted for a minimum of 15 min. The electrical conductivity of the spent NH_4OH solution was measured using an YSI model 3100 conductivity instrument. The washings continued until the electrical conductivity of the spent washes was below 1500 mS/m indicating sufficient amounts of HMTA, urea, and NH_4OH had been removed.

2.2. Carbothermic reduction and nitriding

Process variables for CTRN of the benchmark sol-gel feedstock were investigated and reported in [8]. For this work, a standard time-temperature program was used along with flow rates that fell within the recommended conditions determined in [8]. All experiments were conducted using simultaneous thermal analysis (STA) using a STA 449 F3 Jupiter from NETZSCH-Gerätebau GmbH. The mass loss and standard temperature versus time profile for a run typical of all others is given in Fig. 4. The process gasses were certified to be within their impurity limits (Table 1) by the manufacturer Airgas.

2.3. Test matrix

The sol-gel processing variables investigated in this work are U molarity in the ADUN, carbon source, and the gelation temperature. As mentioned, additives were also introduced into the solution in various forms. Table 2 summarizes each sol-gel feedstock sample studied. Raven 3500 was chosen as the carbon

source to evaluate against the Mogul L benchmark based on a previous investigation [16] of process variables to produce dense UO_2-UC via carbothermic reduction. In that work the sol-gel feedstock contained a molar C/U ratio of 1.28 compared to a slightly higher one ranging from 2.5 – 2.65 for this study.

2.4. X-ray powder diffraction (XRD)

A D2 Phaser, Bruker Inc., X-ray diffractometer with Cu Kα radiation was used for obtaining XRD patterns of the nitride samples. Randomly selected kernels were grinded in a mortar and pestle. The resulting powder was then placed on a zero-background SiO_2 plate on which a slurry of the sample was made using isopropyl alcohol to make a thin and flat layer of the sample which was then covered using Kapton tape as a precautionary measure to fix the radioactive material to the sample holder. An internal standard (Si SRM640d or LaB6 660b) was added while performing the measurement in order to correct for sample displacement. In the case of some samples, the standard material was admixed instead of ubicating it directly on top of the sample. A step size of 0.004° was used in collecting all XRD patterns over ~2h time. Profile fitting was conducted using GSAS software using Rietveld refinement [17].

2.4. Density determinations

Kernel densities were calculated by combining the kernel radii with mean kernel masses. The radii of individual kernels were measured using a shadow-imaging technique for batches of particles (>200) large enough to produce a representative statistical distribution. Individual kernels in these images were segmented out by automated image processing software and the edge coordinates of 720 evenly distributed points around each kernel were identified and used to calculate the mean radius of each kernel. Individual kernel radii were then converted to approximate kernel volumes by assuming that each kernel was a perfect sphere. Finally, these volumes were averaged to determine the mean kernel volume and the associated standard error of the mean.

Average kernel masses were measured in five separate batches of ~200 kernels for each batch of material. Each measurement was performed by weighing a sample of kernels, then counting each kernel in the sample using automated software. The five average kernel mass measurements for each sample were combined into a mean average kernel mass and the associated standard error of that mean was also calculated. These values, combined with the corresponding calculated values for kernel volume, were then used to calculate the mean kernel density and the propagated standard error of that mean. The results of this method were validated against direct measurement of density by mercury porosimetry, and the resulting densities were found to be within each other's error.

3. Results

3.1. Density analysis

The results of the density analysis are presented in Table 2.

3.2. Phase identification and compositional analyses

The XRD pattern shown in Fig. 5 for the UC_xN_{1-x} sample (UNRaven) synthesized using Raven 3500 carbon (C/U = 2.5) without adding any additives indicates only the presence of UN (NaCl type crystal structure with F m -3 m space group) and no secondary phases (e.g., unreacted UO_2). The refined lattice parameter

(p) of this sample was 4.9029±0.0001 Å. Using Eqn. 4 from [8], the composition is therefore $UC_{0.16}N_{0.84}$ (Table 2).

$$x = -759.314 + 3223.5\,p/nm - 3412.4\,p^2/nm^2 \quad (4)$$

The sample (UNLT) synthesized using Mogul L carbon (C/U = 2.650) also contained single phase nitride with a lattice parameter of 4.9072 Å and a calculated chemical composition of $UC_{0.21}N_{0.79}$. The addition of B ((B/U = 0.025) or SiC (SiC/U = 0.201) in the samples synthesized with a C/U molar ratio of 2.5 showed similar lattice parameters and UC_xN_{1-x} chemical compositions with x ~ 0.21. The XRD pattern for UNSiC also showed the presence of relatively low-intense peaks corresponding to reflections of U-Si-based chemical phases (highlighted in Fig. 5). Regardless of the amount of C added in the synthesis, Gd-added (Gd/U up to 0.025) samples (UNGd1 and UNGd3) also showed similar lattice parameters with an approximate composition of $UC_{0.11}N_{0.89}$. In the case of the UNGd2 sample, lattice UN parameter was slightly greater, giving ~$UC_{0.2}N_{0.8}$, than UNGD1 and UNGd3 samples. If desired, in [9] it was demonstrated that the N content can be increased by additional processing in flowing N_2-4%H_2 via removal of the solid-solution C as HCN and substituting N for it on the anion sublattice. An investigation into the required C/U to form high purity UN with no residual UC without the use of this additional step is ongoing.

When Gd/U molar ratio was increased to 0.125, a secondary phase was detected corresponding to cubic Bixbyte-Mn_2O_3 type (I a -3) Gd_2O_3 phase. However, the peak positions of this second phase could also be matched to a fcc-Cu type (F m -3 m) Gd phase, with peaks shifting to the high-angle side. Patterns were collected for two sets of kernels from the sample, and both showed the presence of these reflections. The first set of kernels contained ~13 wt.% Gd, while the second set of kernels contained ~17 wt.%, indicating an inhomogeneous secondary phase distribution. The calculated composition for the two sets of kernels range from $UC_{0.21}N_{0.79}$ – $UC_{0.1}N_{0.9}$. If Gd_2O_3 was used as the second phase, XRD analysis showed its refined lattice parameter to be 10.794 Å, which was smaller than the reported value of 10.8231 Å (ICSD #94892). If Gd was used as the second phase, a lattice parameter of 5.394 Å was obtained, and this value was smaller than the reported value of 5.51 Å (ICSD #20502) for Gd.

As summarized in Table 3, changes in lattice strains could be observed between samples. Those synthesized without the use of any additives had moderate micro-strain values (0.015 and 0.028%). The sample with B also showed similar micro-strain values to those with no additions. The highest micro-strain was obtained for the sample with SiC, while lowest values were obtained for the Gd-added UN samples.

The data indicate that the lattice strain in UC_xN_{1-x} is increased by SiC but relieved by the addition of Gd. The sample with SiC additions showed the presence of secondary U-Si-based phases. Since lattice strain values of samples with Gd were less than that of samples without any additives, it can be inferred that Gd was incorporated to some degree into UN.

EDS elemental mapping was carried out on the samples with Gd additions. Fig. 6 shows U, Gd, N, and O elemental maps for the UNGd4 sample. The mapping shows Gd-rich secondary phases which appear relatively U- and N-free. Most observed Gd-rich secondary phases correspond to increased oxygen intensity relative to the fuel matrix. A few locations showing elevated Gd intensity do not correspond to local increases in oxygen intensity (highlighted by arrows in Gd and O maps). The predominance of

observed Gd-O features relative to Gd features confirms that the secondary Gd-based phase in UNGd4 was mostly Gd_2O_3.

Gadolinium rich areas are less significant in UNGd2 and UNGd3 samples, as only 0.025 molar ratio of Gd/U was used in the samples. Like in UNGd4 sample, many Gd regions areas are partially rich with O, indicating the presence of both Gd and Gd_2O_3 phases (Fig. 7).

The data presented in Table 2 show Gd-added nitride samples consisted of relatively high geometrical densities. Microstructural examination of UC_xN_{1-x} samples without adding Gd contain large number of pores in most kernels, mainly at their centers (Fig. 8a-b). The pore character was less for Gd additions (Fig. 8c-h). The lowest amount of pores (Fig. 8g-h) was observed in the kernels with the highest Gd/U ratio, i.e. UNGd4 (Gd/U = 0.125).

4. Discussion

4.1. Gadolinium additions

The samples with Gd added using $Gd(NO_3)_36H_2O$ showed clear increases in both overall and theoretical density compared to those without it but prepared with the same carbon, dispersant and processing parameters. Gadolinium mononitride and UN are isostructural with both having the same F m -3 m space group; one objective for adding Gd to the feedstock was to form (U,Gd)N in order to take advantage of the known densification mechanisms associated with solid solution sintering [18-21].

The lattice parameter of GdN (4.999 Å, ICSD # 44773) is greater than UN (4.889 Å, ICSD # 44358) because of the larger Gd. Therefore, if (U, Gd)N solid solution was achieved, the UN lattice parameter should be larger than the 4.889 Å. All refined lattice parameters for all samples in the current study are greater than 4.889 Å. Any residual C as U(C,N) can also give rise to an increase in the UN lattice parameter due to larger size of C (atomic radius = 77 pm) than N (atomic radius = 71 pm). A significant increase in lattice parameter over the benchmark however was not observed indicating small GdN solubility in UN or precipitation of a Gd phase upon cooling. The refined lattice parameters of the second Gd phase in the Gd/U sample with a molar ratio of 0.125, was not consistent with Gd metal, GdN, or Gd_2O_3, likely because of U incorporation into the Gd-based phase, at least at small level. At a Gd/U molar ratio of 0.025, XRD did not show the presence of secondary Gd-based phase. However, SEM analysis showed small amounts of Gd-rich areas; thus, the amount of Gd-phase was below the XRD detectable limit. Qualitative analysis using EDS elemental maps showed that the amount of Gd segregated out from the primary UN phase in the UNGd2 (C/U 2.525) sample was greater than that of UNGd3 (C/U 2.500) sample, possibly indicating an impact of C on solubility of GdN in U(C,N). The atomic radius of Gd (180.2 pm) is greater than U (138.5 pm). Since both the calculated lattice parameter from XRD measurements was smaller than both pure Gd and Gd_2O_3, it can be presumed that there is some solubility of U in either Gd or the Gd_2O_3 phase.

The kernels with Gd added as an oxide in the form of Gd_2O_3 nanoparticles to the HMTA/Urea solution showed lower densities compared to both the baseline and those with $Gd(NO_3)_36H_2O$ added to the ADUN. It is proposed that Gd is better mixed as a liquid and thus becomes more randomly distributed when added as $Gd(NO_3)_36H_2O$ compared to Gd_2O_3 nanoparticles. These results suggest sluggish cation interdiffusion between U and Gd. This could help explain the marked difference in results for Gd added as an oxide versus a nitrate hexahydrate. Sluggish cation diffusion supports solid solution sintering as the mechanism as solute drag retards grain growth and promotes densification [18, 20, 22]. Alternatively, when Gd is added as Gd_2O_3, the dispersant effect could be altered resulting in C agglomerations that are

thought to be detrimental to achieving high density kernels [6]. A preliminary run suggests solid solutions with substitutions on the anion sublattice, i.e. C for N, do not appear to enhance densification but this should be the subject of a more in-depth investigation.

4.2. Boron additions

The samples with B showed a decrease in final product density. Boron nitride (BN) exists in a hexagonal structure. It is therefore likely not to exhibit significant solubility in cubic UN. X-ray diffraction analysis shows only the presence of NaCl structure for sample UNB, however, the BN phase was too low to be detected. Its presence cannot be ruled out.

An attempt to incorporate B as B_2O_3 into the uranyl nitrate solution was unsuccessful due to an excessively long gelation time during preliminary testing. It is possible that smaller concentrations of B_2O_3 in combination with another burnable poison additive, like Gd in the form of $Gd(NO_3)_36H_2O$ could be successfully incorporated into the uranyl nitrate and that should be the subject of a future study.

4.3 Silicon carbide additions

Just as B, SiC nanopowder additions resulted in a decrease in final product density. X-ray diffraction analysis shows partially identified peaks that correspond to secondary phases such as U_xSi_y, SiO_2, and $U_xSi_yC_z$. These deleterious secondary phases exert a profound negative influence on densification.

4.5 Other rare earth and thorium additions

It is important to point out that other rare earths and Th are stable as a nitrate and should be amenable to incorporation into the ADUN. These facts permit further studies into how the oxidation state and ionic radii of additives with mononitrides sharing a NaCl structure with UN effect the sintering behavior of UN in general and, in particular, as microspheres from sol-gel feedstock. For example, Eu, like Gd, can be used as a burnable poison and exists as a mixed 2+ and 3+ cation. Thorium is a fertile neutron absorber and the 4+ oxidation state predominates. On the other hand, Pr and Ce can exhibit a mixed 3+ and 4+ valence. An important question to answer is thus: Which of these have the greatest impact on densification and at what metal fraction? Further, any of the lanthanides, Pu, and the minor actinides can be incorporated as nitrates into the ADUN and each are isostructural as a nitride with UN.

4.5. Feed-stock processing variables

Higher density UN microspheres were expected when starting with a denser feedstock. Figure 9 shows this indeed is the trend; however, examination of Table 2 indicates one notable exception is UNGd4. This can be explained by the increased Gd content driving down the overall mass and therefore decreasing the pour density of the sol-gel spheres. However, the presence of Gd significantly enhances the solid solution and/or precipitate densification mechanisms during sintering of the kernels as discussed above.

It was found that the pour density of the sol-gel feedstock can be manipulated by adjusting the Si oil bath temperature as illustrated in Fig. 10. The U concentration variation in the broth showed no apparent effect on results but the gelation temperatures were not held constant. Therefore, a systematic study of U concentration is the subject of continued research.

4.6. Phase equilibria and thermochemistry

Literature concerning the thermodynamics of GdN is limited to first principles studies. Gadolinium nitride was expected to form a solid solution with UN perhaps with complete miscibility; however, the solubility of GdN in UN is either small or Gd precipitates from the UN matrix upon cooling and the Gd rich regions are subsequently oxidized during cross sectioning for ceramography. It could be the case that Gd behaves similarly to UN which decomposes to U liquid metal and N_2 gas at ~3030 °C and 1 atm N_2 pressure [23] but at lower temperatures, i.e. those used for this work (1950°C). If that occurred it could aid in densification through liquid phase sintering (LPS). While the thermodynamics for GdN are ill defined, one can make inferences based on similar rare earth systems. For example, La, Ce, Pr, and Nd as sesquicarbides decompose between 1400 – 1650°C [24]. Further, thermodynamic calculations using the FactSage database show that $p_{N_2} = 2.5 \times 10^{-4}$, 5.6×10^{-4}, 1.3, and 1×10^{-4}atm for YN, LaN, EuN and CeN at 1900°C, conditions close to those for the experiments performed in this work. The p_{N_2} for UN is orders of magnitude lower at 8.8×10^{-6}. An Ar purge of 5 hours at sufficient processing flow rates, as was done in this work, could begin to remove enough N to produce free Gd. On the other hand, the UN would require significantly higher flows and/or longer processing times.

Speidel and Keller [25] reported that vacuum processing of UN at 1650 °C did increase density of UN powder compacts most probably due to an LPS effect since the post-treatment material was a UN-U cermet. For this work, sintering of UN microspheres at 1×10^{-5} mbar was attempted at 1650°C and 1700°C. Figure 11 shows increasing rates of mass loss occurred with increasing temperature as would be expected due to decomposition and evacuation of N_2 gas. The total pressure was well below the equilibrium p_{N_2} of 2.89×10^{-4} and 7.38×10^{-4} atmospheres for the reaction $UN = U^{liq} + N_2$ at 1650°C and 1700°C respectively.[1] However, no statistically significant improvements in density were measured. Therefore, if LPS does occur with Gd additions, the densification likely happens in combination with other phenomena, for example from solute drag and grain boundary growth retardation from secondary phase precipitates.

5. Conclusions

Gadolinium nitrate hexahydrate, Gd_2O_3, B, and SiC can be added to sol-gel derived hydrated uranium oxide feedstock. The most important discovery resulting from this study is the sintering impact Gd can have when introduced as a nitrate hexahydrate to the ADUN. Silicon carbide reacts to form secondary phases and the B is not effective at maintaining or increasing the overall density of the nitride kernel. The type of carbon and dispersant impacts the final density as well.

While the Gd added as $Gd(NO_3)_3 6H_2O$ has been shown to improve the overall density of UN, it also has the effect of displacing U. According to [4], 12.8 g/cm^3 is required for the FCM design. Using the highest density numbers from this study, UNGd2 and UNGd4 result in 12.4 g/cm^3 and 11.8 g/cm^3 respectively. Other routes must be taken to achieve higher U densities, for example hot isostatic pressing which has been shown to produce up UN microspheres with up to13.1 g/cm^3 [28].

---

[1] Calculated using the thermodynamic assessment from [26] P. Y. Chevalier, E. Fischer, B. Cheynet, *J. Nucl. Mater.*, 280 (2000) 136-50. and the FactSage software [27] C. W. Bale, P. Chartrand, S. Degterov, G. Eriksson, K. Hack, R. B. Mahfoud, J. Melançon, A. Pelton, S. Petersen, *CALPHAD*, 26 (2) (2002) 189-228..

A relationship between the sol-gel and final UN microsphere density has been established and the tunable parameter identified, that is the temperature of the Si oil bath. More work is needed to understand how U molarity of ADUN effects densification and will be the subject of future investigations. It was observed that the chemical form of additives, like Gd, had a significant influence on the UN density but not the sol-gel feedstock pour density. Finally, there is a need to assess the thermodynamics of the Gd-N binary and U-Gd-N ternary to support processing of complex UN solutions and/or composites.

Acknowledgements

The authors wish to acknowledge the aid and technical insight of Brian Jolly and Dr. Andrew Nelson at ORNL. This paper was supported by the Advanced Fuels Campaign of the Fuel Cycle R&D program in the Office of Nuclear Energy, US Department of Energy.

The raw/processed data required to reproduce these findings cannot be shared at this time due to technical or time limitations

References

[1] K. A. Terrani, J. Kiggans, Y. Katoh, K. Shimoda, F. C. Montgomery, B. L. Armstrong, C. M. Parish, T. Hinoki, J. D. Hunn, L. L. Snead, *J. Nucl. Mater.*, 426 (1) (2012) 268-76.
[2] K. A. Terrani, L. L. Snead, J. C. Gehin, *J. Nucl. Mater.*, 427 (1) (2012) 209-24.
[3] C. A. Baldwin, J. D. Hunn, R. N. Morris, F. C. Montgomery, C. M. Silva, P. A. Demkowicz, *Nucl. Eng. Des.*, 271 (2014) 131-41.
[4] N. M. George, I. Maldonado, K. Terrani, A. Godfrey, J. Gehin, J. Powers, *Nucl. Technol.*, 188 (3) (2014) 238-51.
[5] C. I. Contescu, T. Burchell, Selection and characterization of carbon black and surfactants for development of small scale uranium oxicarbide kernels, ORNL/TM-2005/548 (2005)
[6] M. Ebner, Chemistry Improvement for the Production of LEU UCO Fuel Using Manufacturing Scale Equipment–FY 2004 Final Report, Idaho National Laboratory, INEEL/EXT-04-02372 (2004)
[7] M. A. Ebner, C. M. Barns, UCO Kernel Fabrication Development for the Advanced Gas Reactor Program, Idaho National Laboratory INL/EXT-07-12247 (2007)
[8] T. Lindemer, C. Silva, J. Henry, J. McMurray, S. Voit, J. Collins, R. Hunt, *J. Nucl. Mater.*, 483 (2017) 176-91.
[9] T. B. Lindemer, C. M. Silva, J. J. Henry Jr, J. W. McMurray, B. C. Jolly, R. D. Hunt, K. A. Terrani, Carbothermic Synthesis of~ 820-μm UN Kernels: Investigation of Process Variables, Oak Ridge National Laboratory (ORNL), Oak Ridge, TN (United States), Report ORNL/TM-2015/301 (2015)
[10] R. A. Lowden, Fabrication of Baseline and Variant Particle Fuel for AGR-1, Oak Ridge National Laboratory, Oak Ridge, TN, ORNL Report No. CF-06/02 (2006)
[11] D. A. Petti, J. T. Maki, J. D. Hunn, P. J. Pappano, C. M. Barnes, J. J. Saurwein, S. G. Nagley, J. M. Kendall, R. R. Hobbins, *JOM*, 62 (9) (2010) 62-6.
[12] J. A. Phillips, C. M. Barnes, J. D. Hunn, *Proceedings of HTR 5th International Topical Meeting on High Temperature Reactor Technology, Prague, October 18-20*, 2010 (2010)
[13] J. Collins, R. Hunt, *ORNL/CF-05/07*, (2005)
[14] J. Collins, M. Lloyd, R. Fellows, *Radiochim. Acta*, 42 (3) (1987) 121-34.
[15] P. A. Haas, J. M. Begovich, A. D. Ryon, J. S. Vavruska, *Industrial & Engineering Chemistry Product Research and Development*, 19 (3) (1980) 459-67.
[16] R. D. Hunt, J. A. Johnson, J. L. Collins, J. W. McMurray, T. J. Reif, D. R. Brown, *J. Nucl. Mater.*, 498 (2018) 269-73.
[17] A. Larson, R. Von Dreele, General Structure Analysis System (GSAS), Los Alamos National Laboratory, LAUR 86-748 (2000)
[18] R. Brook, *Sci. Sintering*, 20 (2) (1988) 115-8.
[19] C. B. Carter, M. G. Norton, *Ceramic materials: science and engineering*, Springer Science & Business Media, 2007.
[20] L. C. De Jonghe, M. N. Rahaman, *Handbook of Advanced Ceramics: Materials, Applications, Processing and Properties*, 2 (2003) 187.
[21] M. Harmer, *Advances in ceramics*, 10 (1984) 679.
[22] M. Rahaman, Y. Zhou, *J. Eur. Ceram. Soc.*, 15 (10) (1995) 939-50.
[23] W. Olson, R. Mulford, *The Journal of Physical Chemistry*, 67 (4) (1963) 952-4.
[24] K. Gschneidner, F. Calderwood, *Bulletin of Alloy Phase Diagrams*, 7 (5) (1986) 421-36.
[25] E. O. Speidel, D. L. Keller, Fabrication and properties of hot-pressed uranium mononitride, Battelle Memorial Inst.; Columbus, Ohio, BMI-1633; EURAEC-706 (1963)
[26] P. Y. Chevalier, E. Fischer, B. Cheynet, *J. Nucl. Mater.*, 280 (2000) 136-50.
[27] C. W. Bale, P. Chartrand, S. Degterov, G. Eriksson, K. Hack, R. B. Mahfoud, J. Melançon, A. Pelton, S. Petersen, *CALPHAD*, 26 (2) (2002) 189-228.
[28] J. W. McMurray, J. Kiggans, K. Terrani, Examination of HIP for production of high density UN kernels, Oak Ridge National Laboratory, ORNL/SR-2017/155 (2017)

[29] J. W. McMurray, R. Hunt, C. M. Silva, G. Helmreich, K. Terrani, Examination of viability of UN kernel production with additives such as SiC and B, Oak Ridge National Laboratory, ORNL/SPR-2017/386 (2017)
[30] J. W. McMurray, J. O. Kiggans, G. W. Helmreich, K. A. Terrani, *J. Am. Ceram. Soc.*, (2018)
[31] J. W. McMurray, C. M. Silva, G. Helmreich, T. Gerczak, J. A. Dyer, J. L. Collins, R. Hunt, T. Lindemer, K. Terrani, Production of Low Enriched Uranium Nitride Kernels for TRISO Particle Irradiation Testing, Oak Ridge National Laboratory (ORNL), Oak Ridge, TN (United States), ORNL/SR-2016/268 (2016)

Table 1. Impurity limits for the process gases used for the sol-gel feedstock to UN conversions.

Impurity	**UHP Ar**	**UHP N_2**
Moisture	< 3 ppm	< 3 ppm
O_2	< 2 ppm	< 2 ppm
Hydrocarbons	< 0.5 ppm	< 0.5 ppm
CO_2	< 1 ppm	< 1 ppm
CO	< 0.5 ppm	< 1 ppm
N_2	< 5 ppm	99.999%

Table 2. Details of the feedstock along with the phases present, the overall density, C/U, C/M (where M = U + Gd or U + B) and composition of corresponding $UC_{1-x}N_x$ kernels as determined from XRD. Note, SEM shows Gd as a second phase precipitate in UNGd-2. Compositions are also reported for some samples.

Sample	Feed stock molar ratios	U molarity	Pour density g/cc	Si oil temp.	Carbon/dispersant	Additive	Density g/cc	XRD analysis
UNB	C/M – 2.500 B/U – 0.025	1.3	0.88	60°C	Cabot/Tamol	B-10 as <22µm powder	12.40±0.17	Phases – UN LP – 4.9074 $UC_{0.21}N_{0.79}$
UNGd-1	C/M – 2.590 Gd/U – 0.025	1.3	0.95	60°C	Cabot/Tamol	Gd as Gd_2O_3 nanopowder	9.64±0.11†	Phases – UN LP – 4.8991 $UC_{0.11}N_{0.89}$
UNGd-2	C/M – 2.525 Gd/U – 0.025	1.3	1.00	60°C	Cabot/Tamol	Gd as $Gd(NO_3)_36H_2O$	13.41±0.08	Phases – UN LP – 4.9074 & 4.9079 Avg. $UC_{0.20}N_{0.80}$
UNSiC	C/M – 2.500 SiC/U – 0.201	1.3	1.00	60°C	Cabot/Tamol	SiC powder	11.39††	Phases – UN LP – 4.9069 $UC_{0.21}N_{0.79}$
UNRAVEN	C/U – 2.500	1.36	0.98	70°C	Raven 3500/Tamol	none	13.19±0.14	Phases – UN LP – 4.9029 $UC_{0.16}N_{0.84}$
UNLT	C/U – 2.650	1.3	0.88-0.96‡	60°C	Cabot/Tamol	none	12.84±0.07	Phases – UN LP – 4.9072 $UC_{0.21}N_{0.79}$
UNMT	C/U – 2.650	1.2	1.04	65°C	Cabot/Tamol	none	12.97±0.05	TBD
UNHT	C/U – 2.650	1.1	0.93	80°C	Cabot/Tamol	none	12.89±0.05	TBD
UNGd-3	C/M – 2.500 Gd/U – 0.025	1.36	0.96	70°C	Raven 3500/Tamol	Gd as $Gd(NO_3)_36H_2O$	12.9±0.21	Phases – UN, Gd_2O_3 LP – 4.8997 $UC_{0.11}N_{0.89}$
UNGd-4	C/M – 2.500 Gd/U – 0.125	1.36	0.87	70°C	Raven 3500/Tamol	Gd as $Gd(NO_3)_36H_2O$	13.66±0.22	Phases – UN LP – 4.8994 & 4.8980 Avg. $UC_{0.11}N_{0.90}$

†Average diameter of 10-30 microspheres computed from weights and diameters measured with an optical microscope.
††Density determined using Archimede's principle.
‡Typical ranges for the standard batch from [28-31] established from experience.

Table 3. Crystallographic information of selected UN samples.

Sample	UN L.P.	μstrain (%)
UNF-70-3500	4.9029	0.015
UNLT	4.9072	0.028
UNB	4.9074	0.027
UNSiC	4.9069	0.237
UNGd-1	4.8991	0.003
UNGd-4	4.8994	0.002

Figure 1. Comparison between the conventional oxide fuel rod and the LWR FCM fuel concept. Reprinted from Journal of Nuclear Materials, Volume 426, Issues 1-3, Terrani et al., Fabrication and characterization of fully ceramic microencapsulated fuels, 268-276., Copyright (2012), with permission from Elsevier.

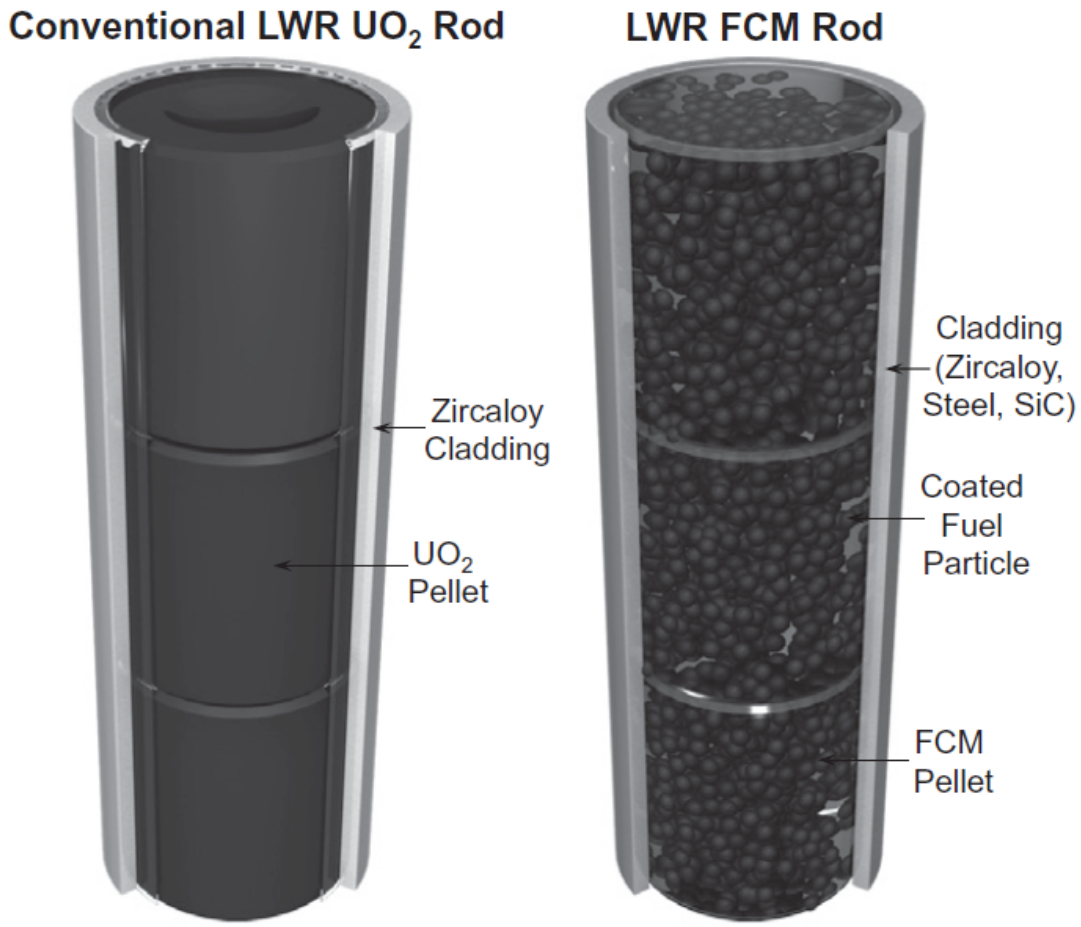

Figure 2. Cross-sectioned FCM TRISO particle.

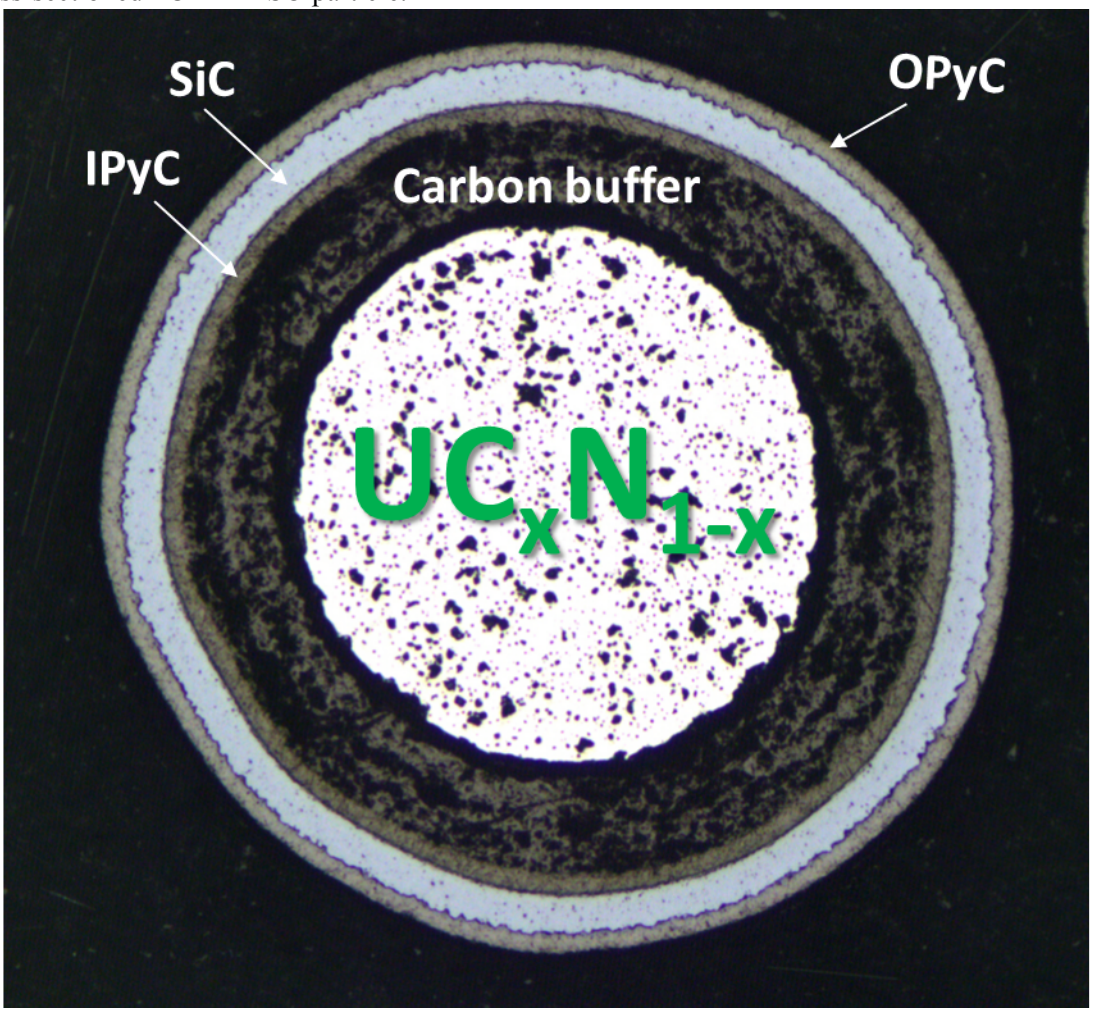

Figure 3. Flow chart of the integral FCM TRISO particle process

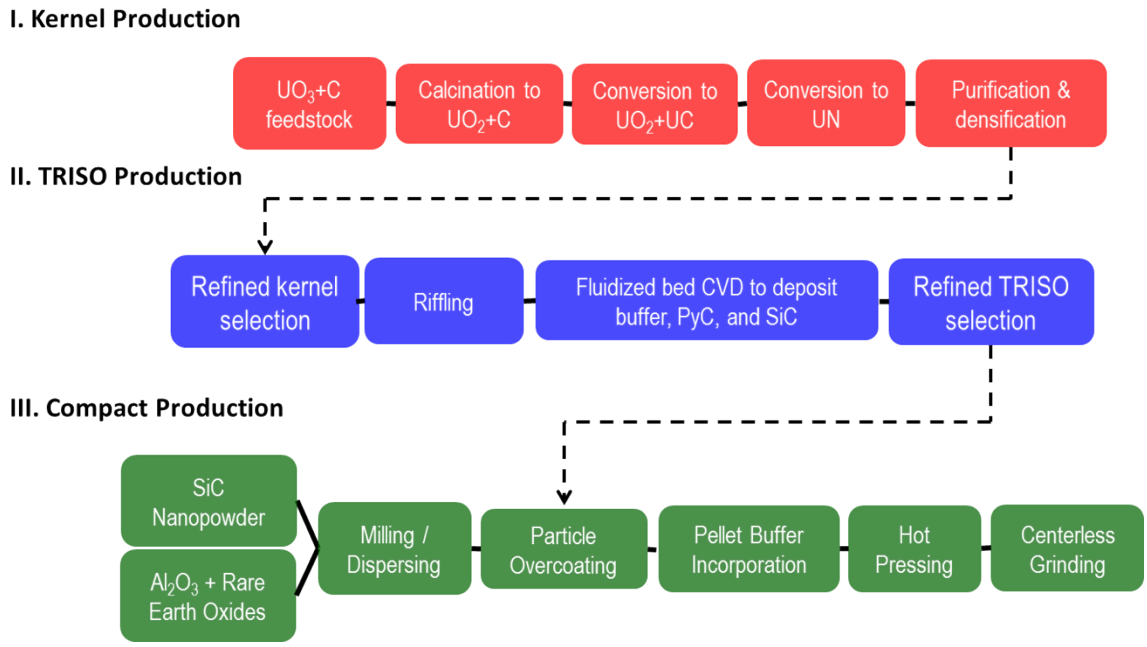

Figure 4. Solid line is the typical % mass loss from thermogravimetry (TG) for the standard temperature (dashed) versus time carbothermic reduction and nitriding program.

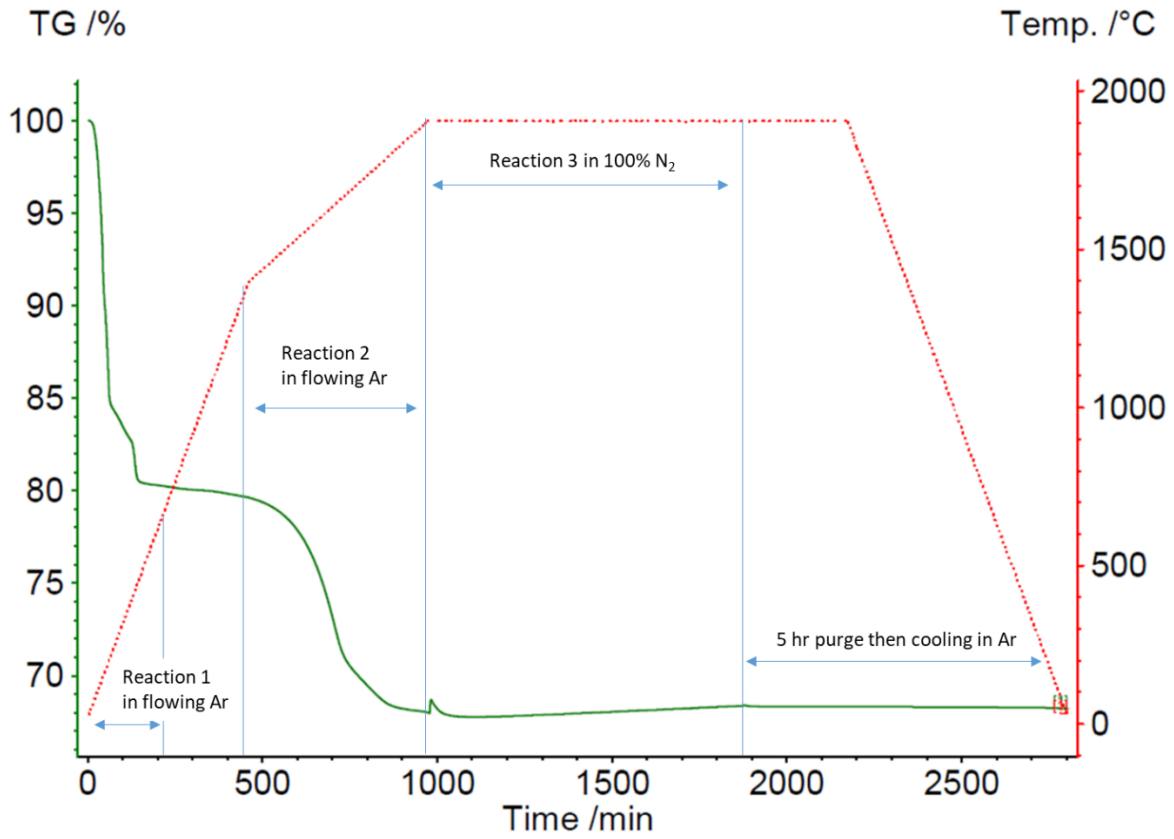

Fig. 5. Powder XRD patterns of selected uranium nitride samples. Asterisks depict peak positions for secondary U-Si-based chemical phases. Bragg reflections only in 27 – 70° range are shown for clarification.

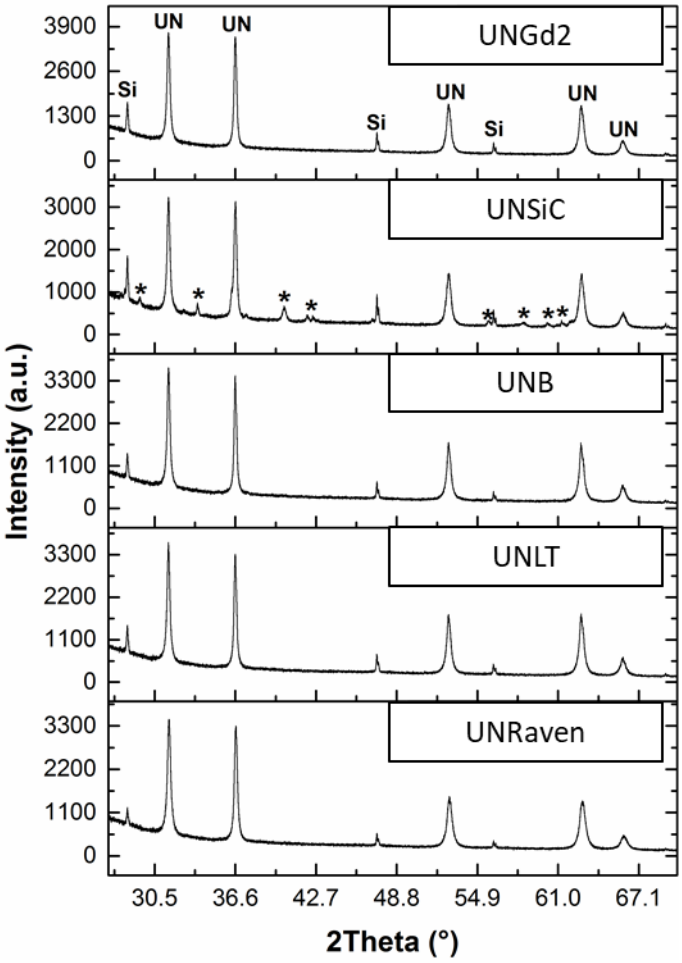

Figure 6. SE-SEM micrograph and EDS elemental maps of a selected region of UNGd4 sample. Bottom-left shows a composite U-Gd-O elemental map. A few O-free and Gd-rich grain areas are highlighted by arrows in Gd and O maps.

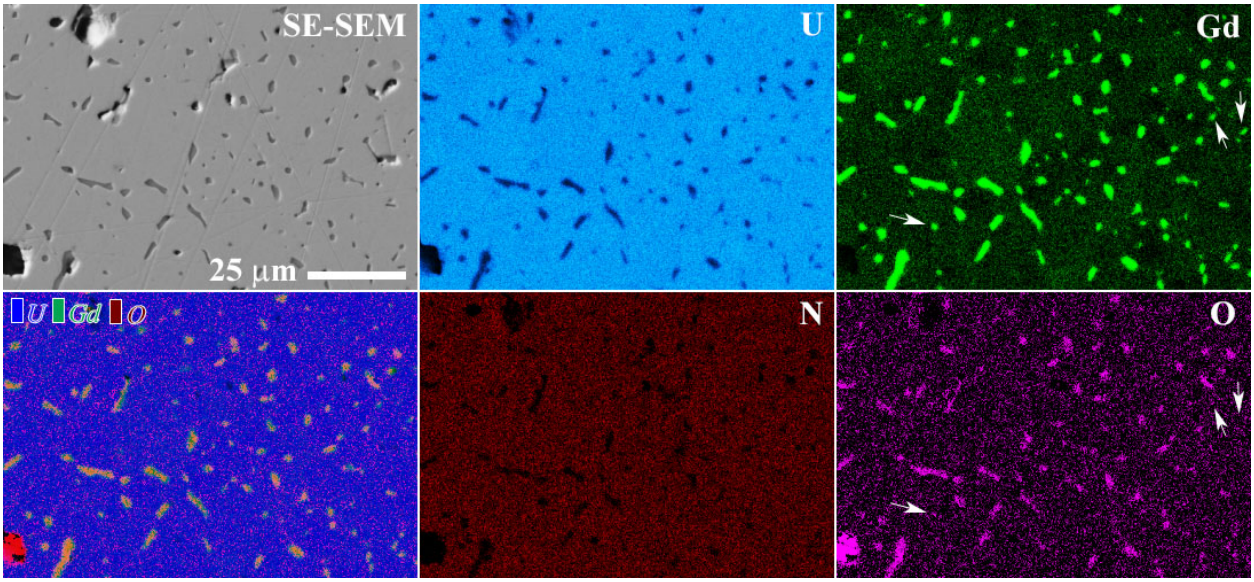

Figure 7. SE-SEM micrographs of selected areas of UNGd2 (top) and UNGd4 (bottom) samples. The corresponding U, Gd, O, and N EDS elemental maps are also shown.

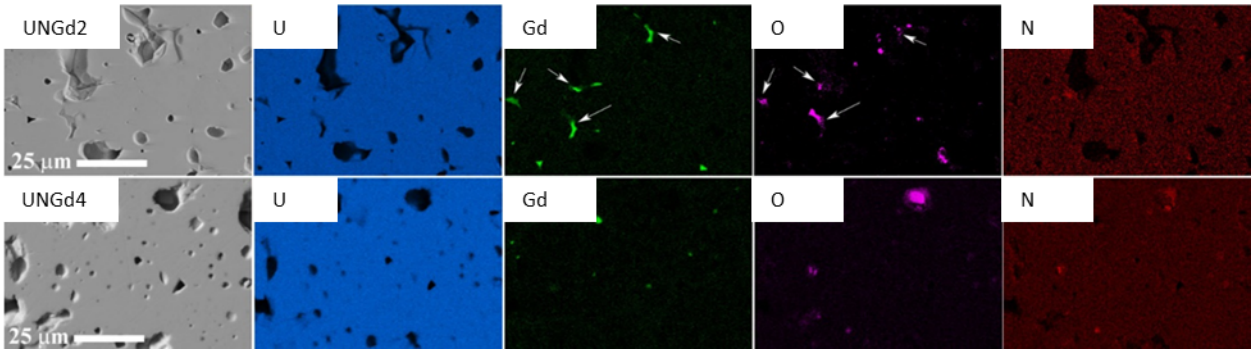

Figure 8. Typical microstructures of FCM-UN1 (a-b), UNGd-2 (c-d), UNGd-3 (e-f), and UNGd-4 (g-h) samples. High-resolution micrographs in each case was obtained focusing the center of the samples.

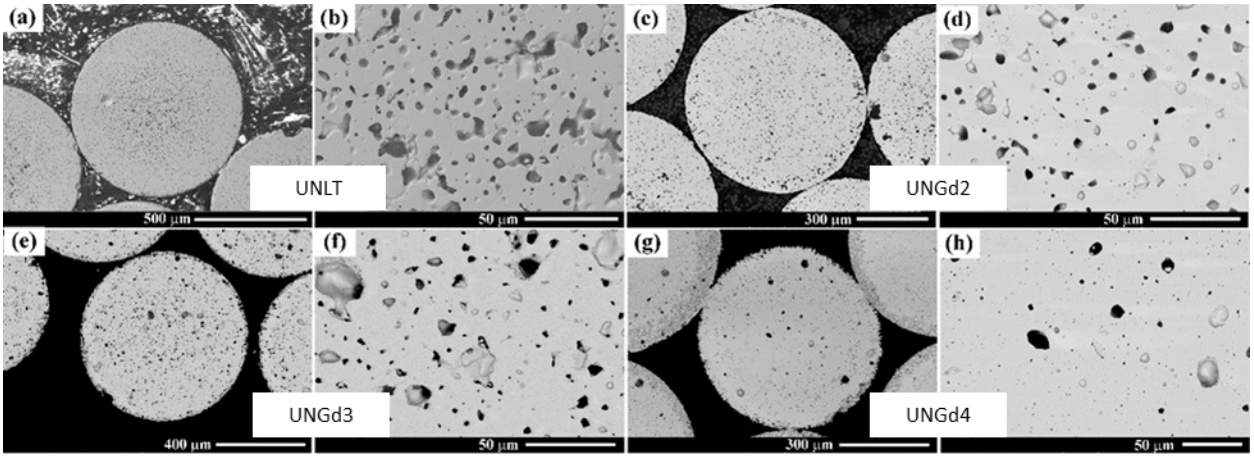

Figure 9. Pour vs kernel density for microspheres with no additives.

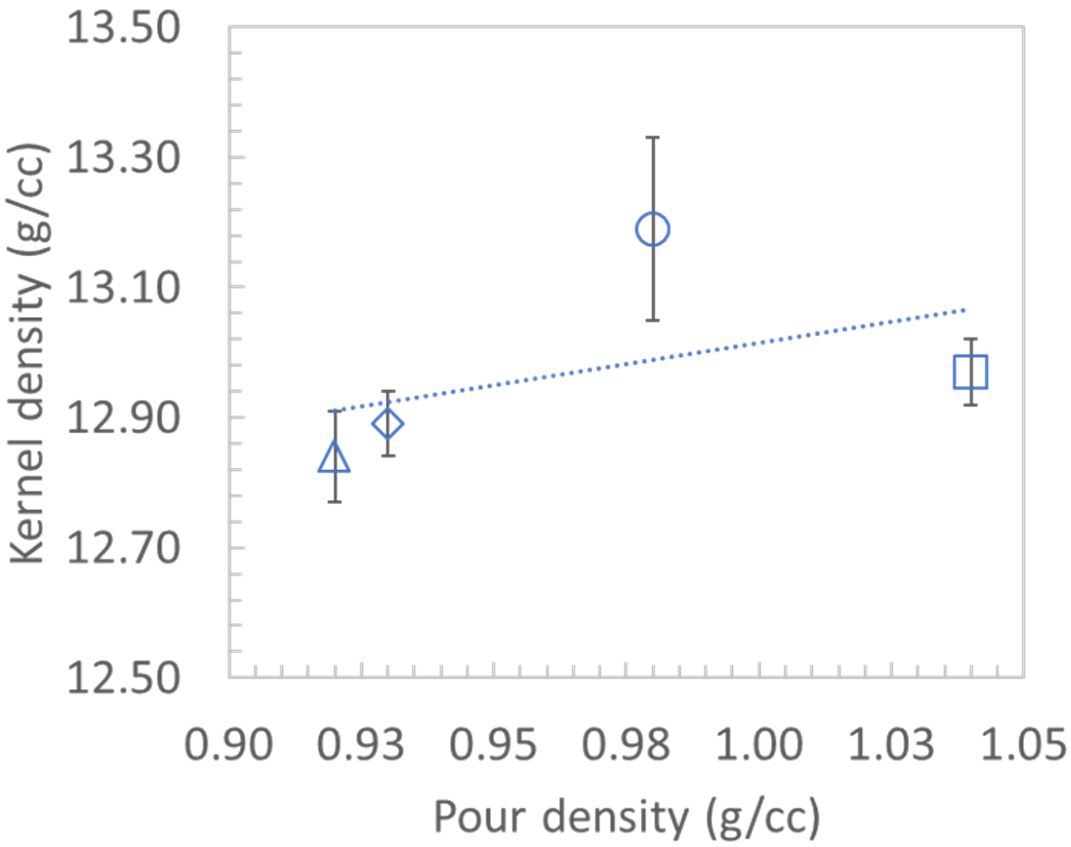

Figure 10. Silicon oil bath (gelation) temperature effect on the pour density of the ~1700 µm spherical sol-gel feedstock

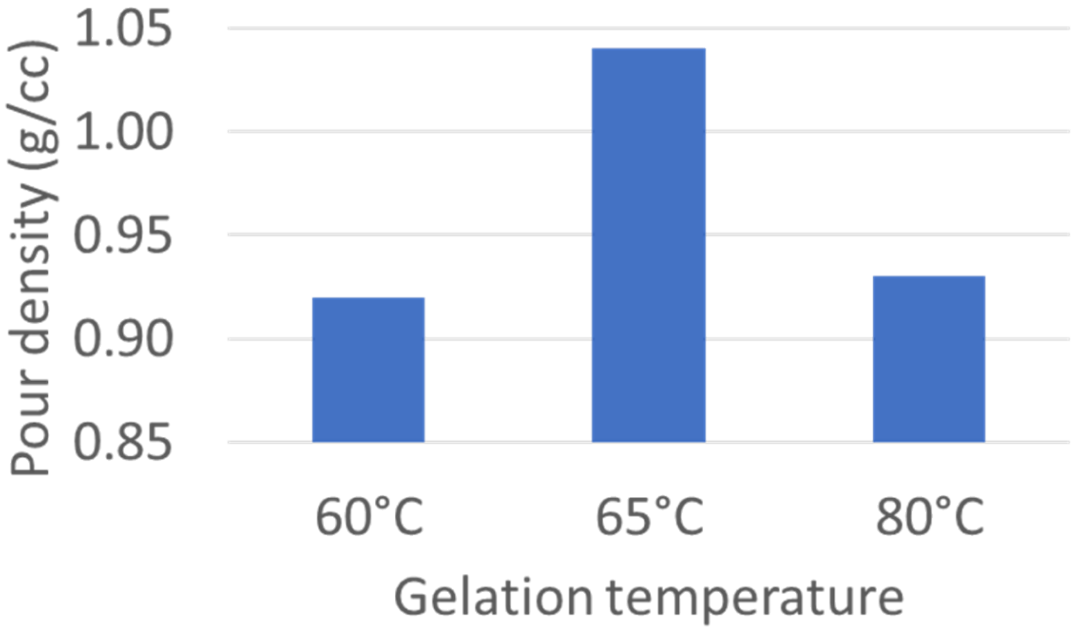

Fig. 11. Percent mass loss from thermogravimetry (TG) versus time for isothermal holds at 1650°C (dotted lines) and 1700°C (solid lines) in a Netzsch Jupiter 449 F3 STA.